Lithos 228–229 (2015) 78–89

Contents lists available at ScienceDirect

Lithos

journal homepage: www.elsevier.com/locate/lithos

Fluid-present deformation aids chemical modification of chromite: Insights from chromites from Golyamo Kamenyane, SE Bulgaria

Takako Satsukawa [a,*], Sandra Piazolo [a], José María González-Jiménez [a,b], Vanessa Colás [a,c], William L. Griffin [a], Suzanne Y. O'Reilly [a], Fernando Gervilla [d], Isabel Fanlo [c], Thomas N. Kerestedjian [e]

[a] Australian Research Council Centre of Excellence for Core to Crust Fluid Systems/GEMOC, Department of Earth and Planetary Sciences, Macquarie University, Sydney, NSW 2109, Australia
[b] Departamento de Geología and Andean Geothermal Center of Excellence (CEGA), Facultad de Ciencias Físicas y Matemáticas, Universidad de Chile, Santiago, Chile
[c] Departamento de Ciencias de la Tierra, Universidad de Zaragoza, Pedro Cerbuna 12, 50009 Zaragoza, Spain
[d] Departamento de Mineralogía y Petrología and Instituto Andaluz de Ciencias de la Tierra, Universidad de Granada-CSIC, Avda. Fuentenueva s/n, 18002 Granada, Spain
[e] Geological Institute, Bulgarian Academy of Sciences, 24 Georgi Bonchev Str., 1113 Sofia, Bulgaria

ARTICLE INFO

Article history:
Received 28 November 2014
Accepted 25 April 2015
Available online 9 May 2015

Keywords:
Chromite
Crystal-plastic deformation
Chromite recrystallization
Metamorphic modification
Fluid present deformation

ABSTRACT

Chemical signatures of chromitites are commonly used to track the evolution of the Earth's mantle. However, chemical modification during deformation may have important implications for the interpretation of chromites' signatures. Here, we describe the details of how deformation promotes chemical modification in chromite. Physicochemical characteristics of the chromites were quantified by measuring crystallographic orientation relationships using Electron Back-Scattered Diffraction (EBSD) and electron microprobe analysis (EMP). Chromites show porphyroclastic textures with coarse-grained porphyroclasts (ca. 0.2–5 mm) and fine-grained neoblasts (<200 μm). Coarse-grained chromites are chemically zoned in terms of major elements from core to rim, preserving this initial igneous feature in the cores, while the outer rims reveal a metamorphic signature. Large chromite grains are characterized by local crystal-plastic deformation, exhibiting distinct inter-crystalline deformation including continuous crystal bending and subgrain boundaries as well as chemical modification in their outer, deformed parts. Two types of fine-grained chromite, F1 and F2, are present. While F1 exhibits a well-developed polygonal texture, straight grain boundaries and low intercrystal misorientation (<1°), F2 shows low-angle boundaries and significant intercrystalline misorientation (2–8°). Both F1 and F2 have higher Fe^{3+} and Cr and lower Mg# values than the cores of large grains. We interpret F1 and F2 to represent chromite recrystallized by heterogeneous nucleation and subgrain rotation recrystallization, respectively. Crystallographic preferred orientation (CPO) and misorientation data on the well-developed low-angle (subgrain) boundaries in coarse grains and F2 grains indicate that deformation in chromite was accommodated mainly by dislocation creep with the dominant activation of the {111}<100> slip system. The retrograde P–T exhumation path predicted by thermodynamic and chemical modeling suggests that these fine-grained chromites were produced when the initial chromitites reacted with oxidizing fluids during retrograde metamorphism (~1.0 GPa and 500–700 °C). Our results show that deformation in the dislocation-creep regime in a chemically open system has induced chemical modification and homogenization within chromite aggregates as well as strain localization. This close physicochemical link offers new avenues of interpreting the chemical signatures of chromites, utilizing their microstructurally controlled variation or lack thereof.

1. Introduction

Chromite is one of the main reservoirs of chromium in the Earth (e.g. Arai, 1992, 1997; Barnes and Roeder, 2001; Stowe, 1994). It is an essential phase in the mineral assemblage of the upper mantle peridotites preserved in ophiolites, where it can be concentrated in bodies known as chromitites (e.g., González-Jiménez et al., 2014). Scientific interest in chromite arises from the fact that within peridotitic rocks, chromites in general are better preserved than silicates, as they are more resistant to fluid-related processes; this has led to the widespread use of chromitites to track the evolution of the Earth's mantle convection (e.g. Arai, 2010; González-Jiménez et al., 2012, 2014; Miura et al., 2012; Walker et al., 2002). Chromitites in ophiolites are commonly hosted within discordant or subconcordant dunite bodies, within the shallow mantle part of the oceanic lithosphere (e.g. Arai and Abe, 1995; Arai and Yurimoto, 1994; Gervilla et al., 2005; González-Jiménez et al., 2014; Melcher et al., 1997; Proenza et al., 1999; Zhou et al., 1994, 1996).

A global chromitite cycle from crust to mantle and back again has been suggested by geochemical studies (Arai, 2013; McGowan et al.,

* Corresponding author. Tel.: +61 2 9850 8346; fax: +61 2 9850 8943.
E-mail address: takako.satsukawa@mq.edu.au (T. Satsukawa).

http://dx.doi.org/10.1016/j.lithos.2015.04.020
0024-4937/

2015, and references therein). Utilizing chemical signatures without direct investigation of the possible deformation features may result in a biased interpretation, as it has been demonstrated for other minerals that the chemical signature may be significantly influenced by deformation (e.g. Büttner, 2005; Erickson et al., 2015; Kruse and Stünitz, 1999; McCaig et al., 2007; Pearce and Wheeler, 2010; Timms et al., 2006). Hence, for improved interpretation and a realistic understanding of the various chemical signatures commonly observed in metamorphosed chromites, it is crucial to understand in depth the link between chemical signature and deformation. However, the assessment of the deformation mechanisms affecting chromite chemical signatures has been hampered, because such a study requires us to distinguish grains and subgrains, to quantify the preferred orientation of chromite, and to link chemical changes to these crystallographic relationships. Because chromite is isotropic, it has been difficult to derive crystallographic relationships in chromite aggregates via optical microscopy.

With the advent of advanced microanalytical techniques, it is now possible to study deformation of chromite in detail; detailed analysis of orientation relationships can be achieved through Electron Back-Scattered Diffraction (EBSD) analysis (Prior et al., 1999). Recently, the EBSD technique has been used to study chromite crystallographic relationships (Prichard et al., 2015; Vukmanovic et al., 2013); neither of these studies has discussed the details of possible deformation processes. Besides the potential influence of deformation on chemical signatures, the identification and characterization of deformation mechanisms in chromite-rich zones are of interest because these mechanisms govern the rheological response of chromite-dominated rocks (e.g. Frost and Ashby, 1982). Deformation mechanisms such as plastic deformation including diffusion creep (Christiansen, 1985; Ozawa, 1989), dissolution followed by precipitation in the presence of melt, and/or dislocation creep (Secher, 1981) are expected to play a role in the modification of chromite microstructures, but have so far commonly been overlooked due to the analytical problem noted above.

Dislocation creep is not thought to be a dominant mechanism; instead, diffusional creep, which normally does not produce an oriented crystallographic fabric, was considered to be the principal mechanism in the deformation of chromites (Ozawa, 1989). In deformed ophiolitic chromitites, large grains are commonly perfect without bending of the lattice or internal substructures (e.g. subgrains), and no crystallographic preferred orientation of chromite has been detected using the X-ray goniometer (Christiansen, 1985). These features have been interpreted to indicate that chromite mainly deforms by passive rotation in the weaker silicate matrix, and by cataclasis and/or diffusion creep (Christiansen, 1985).

However, microstructural work on chromites in ophiolites from Oman, Vourinos (Greece) and Tiebaghi (New Caledonia) (Christiansen, 1986) utilizing electron channeling patterns in scanning electron microscope (SEM) showed that dislocation creep is active in chromite deformed at high temperatures under mantle conditions. Nevertheless, Christiansen (1986) implied that diffusion-accommodated flow is significant and mechanisms related to dislocation structures only provide a secondary mode of deformation compared to brittle fracturing and passive rotation of chromite grains and fragments in the weaker (silicate) matrix.

Few other studies have investigated the deformation of chromite in chromitites (Ghosh and Konar, 2012; Ghosh et al., 2014; Huang et al., 2004), and these were limited to microscopic observations of the transition from brittle to crystal-plastic flow. Recent observations from back-scattered electron (BSE) images obtained using SEM as well as electron microprobe (EPMA) have identified substructures in ophiolitic chromites, and suggest that in general dislocation processes may be active in chromite deforming at high temperatures during mantle flow (Ghosh et al., 2013, 2014). However, these authors did not provide the required key detailed orientation data and information on slip system activation.

This paper presents an EBSD study combined with chemical mapping and spot analysis of natural chromite samples from chromitites hosted in the serpentinite body of Golyamo Kamenyane, in south Bulgaria (Colás et al., 2014; Gervilla et al., 2012). These chromitites have undergone deformation concomitant to fluid–rock interaction during metamorphism, and previous work suggested that these chromitites are one of the most chemically modified and deformed examples (Colás et al., 2014). We document how chromite has deformed under fluid-present amphibolite-facies conditions, providing new insights into the microstructural evolution of chromite during retrograde metamorphism. The results show how, during deformation, the chemical signature of chromite is markedly modified, suggesting that studies utilizing chromite chemistry to infer conditions at high PT and a specific chemical environment need to take into account the effects of deformation on the chemical signature.

2. Geological setting and samples

The studied chromitites are enclosed in serpentinized peridotites of the Golyamo Kamenyane massif, which is part of a dismembered ophiolite complex in the upper unit of the metamorphic basement of the Eastern Rhodopes crystalline massif in southern Bulgaria (Bonev, 2006; Haydoutov et al., 2004; Kolcheva et al., 2000) (Fig. 1). According to recent investigations, the ultramafic rocks of the Eastern Rhodopes have undergone ultra-high pressure (UHP)/high temperature (HT) metamorphism (>2.5 GPa and >1200 °C), and a later overprint at eclogite- or granulite-facies (1.4–1.6 GPa and 750–775 °C). A later amphibolite-facies (~1.0 GPa and 600–650 °C) overprint is also recorded in metasediments spatially associated with the mantle rocks (e.g. Mposkos and Krohe, 2006; Mposkos, 2002). Mposkos et al. (2011) have estimated a similar retrograde metamorphic pathway in the rocks of the adjacent Gneiss Migmatite Complex: from ultra-high pressure (2.1–2.3 GPa) with lower temperatures (533–617 °C), to eclogite-facies (1.5–1.9 GPa and 566–672 °C) and then an amphibolite-facies overprint (0.7–0.9 GPa and 498–570 °C).

Gervilla et al. (2012) suggested that during the retrograde metamorphism, primary chromite of the chromitites from Golyamo Kamenyane reacted with the olivine matrix in the presence of low fO_2 fluids and subsequently with oxidizing Fe^{3+}-rich fluids. This two-stage alteration process produced two distinct features in the chromite grains:

1) Partial to complete replacement of original grains of chromite by a secondary Fe^{2+}-rich porous chromite due to the infiltration of fluids with very low fO_2 at temperatures from ~450 to ~700 °C:
2) Alteration of the chromitites in a late oxidizing hydrothermal event at temperatures below 600 °C, which produced homogeneous (non-porous) ferrian chromite (i.e., Fe^{3+}-rich chromite). This late alteration is confined to localized high-strain zones in the chromitite body.

In this study, we have investigated chromitites classified as zoned and homogeneous (non-porous) chromites according to Gervilla et al. (2012), which were affected by amphibolite-facies tectonometamorphism in the presence of oxidizing Fe^{3+}-rich fluids. These chromites are taken from a late, local high-strain zone (Fig. 1) interpreted to have formed during the retrograde tectonometamorphic event (Colás et al., 2014).

3. Analytical methods

Microstructural analyses including grain size, grain shape and crystallographic relationships and chemical compositions in major elements were conducted by Electron Back-Scattered Diffraction (EBSD), electron microprobe (EMP), and energy dispersive X-ray spectroscopy (EDS), respectively.

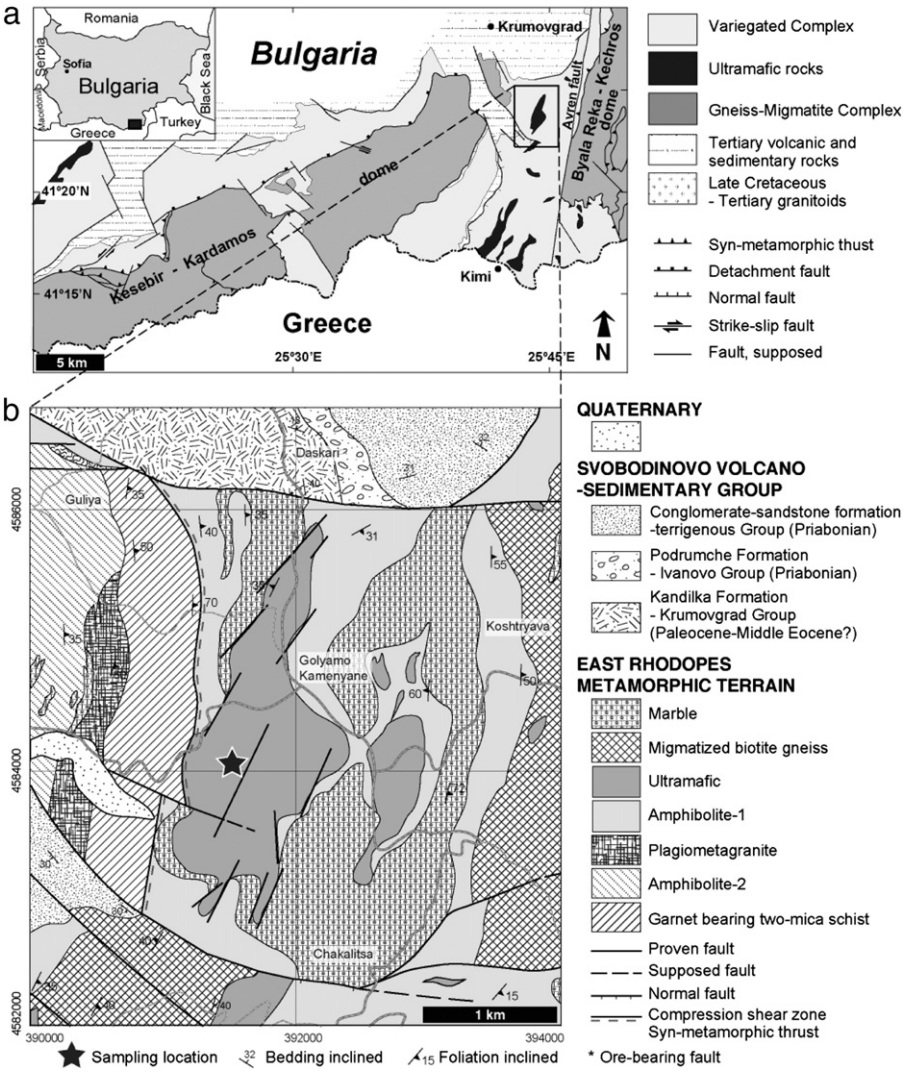

Fig. 1. (a) Location of the Eastern Rhodope Massif. (b) Simplified geological map of the Eastern Rhodope. Black star represents the sampling location. Locality map of the Golyamo Kamenyane serpentinite and nearby areas (modified from Bonev, 2006).

3.1. Microstructural analysis (EBSD and EDS)

To evaluate the characteristics of the chromite fabric and determine active deformation mechanisms, crystallographic orientations were measured using the SEM-EBSD facility coupled with semi-quantitative EDS analysis in the Geochemical Analysis Unit (GAU) Facility of the ARC (Australian Research Council) Centre of Excellence for Core to Crust Fluid Systems (GEMOC, Macquarie University, Australia). The EBSD patterns were generated by the interaction of a vertical incident electron beam with a polished thin section, tilted at 70° to the horizontal in a scanning electron microscope (Zeiss EVO MA15). The operating conditions were a voltage of 20 kV, a current of 8.2 nA and working distance of 12–13 mm. The diffraction pattern was projected onto a phosphor screen and recorded using a digital CCD camera. The resulting image was then processed and indexed in terms of crystal orientation using the CHANNEL5 software distributed by Oxford Instruments. Maps were acquired with sampling step size of 3 μm. Data treatment allowed the rare non-indexed pixels to be filled, if up to six identical neighbors existed with this orientation. We present the resulting data in the form of color-coded maps and pole figures. For the maps that show crystal orientation changes relative to the specific direction of the sample reference frame, full red, green and blue colors are assigned to the grains whose <100>, <110> or <111> axes are parallel to the projection of the inverse pole figure. Intermediate orientations are colored as a mixture of the primary axes. For our analysis, we define (i) a grain as an area that is completely surrounded by boundaries with a misorientation of 10, (ii) a grain size of equivalent circle diameter calculated by grain area, (iii) the mean misorientation of a grain as the average misorientation of 1000 randomly picked orientation pairs within an individual grain, and (iv) the local misorientation of a pixel as its average misorientation considering the orientation of its direct neighbors. Consequently, a grain can exhibit subgrain boundaries.

We use the boundary trace analysis to determine the geometry of low-angle boundaries and the active slip system(s) from the EBSD data. When the 3D orientation of a boundary is unknown, the boundary trace analysis provides a crystallographically consistent solution for the boundary geometry, if ideal tilt and twist boundary models are assumed. This method considers the dispersion of the orientation data around a rotation axis for an area sampled across a selected 2D trace of a low-angle boundary on EBSD maps. The rotation axis is identified on the pole figures as the direction with no or little dispersion (Lloyd and Freeman, 1994). In the case of a tilt boundary, the boundary plane must contain the 2D boundary trace and the rotation axis. A plane at a high angle (ideally at 90°) to the boundary plane and containing the rotation axis represents the most likely active slip plane and must contain the slip direction. In the case of a twist boundary, the rotation axis is perpendicular to the boundary plane. Boundary trace analysis has been used successfully in EBSD studies of various geological materials: quartz

(e.g. Lloyd et al., 1997; Menegon et al., 2011), halite (Borthwick and Piazolo, 2010), calcite (Bestmann and Prior, 2003), garnet (Prior et al., 2002), kyanite (Beane and Field, 2007), sillimanite (Piazolo and Jaconelli, 2013), zircon (e.g. Piazolo et al., 2012; Reddy et al., 2007), pyrite (Barrie et al., 2008) and water ice (Piazolo et al., 2008).

3.2. Mineral chemistry (EMP)

A preliminary qualitative analysis of variations in chemical composition was achieved by BSE imaging, where variations in the gray scale signify minor chemical changes. The chemical compositions of the different zones identified by BSE imaging were analyzed quantitatively using a CAMECA SX-50 electron microprobe at Serveis Científico Técnics of University of Barcelona (Spain). Operating conditions were 20 kV accelerating voltage and a beam current of 20 nA probe current, with a beam of 3 μm in diameter. Counting times were 20 s on TAP/PET and 30 s on LiF crystals. ZAF corrections were applied online. Monitored spectral lines were Mg Kα, Al Kα, Si Kα, Ti Kα, Cr Kα, V Kα, Mn Kα, Fe Kα, Ni Kα and Zn Kα. Standards used were: periclase (Mg), Al_2O_3 (Al), Cr_2O_3 (Cr), Fe_2O_3 (Fe), diopside (Si), rutile (Ti), pure V, rhodonite (Mn), NiO (Ni), and sphalerite (Zn). Ferrous and ferric iron contents of chromite were calculated assuming ideal spinel stoichiometry and structural formulae were calculated following the procedure of Droop (1987). Data are reported in Supplementary Table 1. Cr# was calculated as equal to Cr/(Cr + Al) atomic ratio, and Mg# was the Mg/(Mg + Fe^{2+}) atomic ratio.

4. Results

4.1. Microstructure

Chromitites show a porphyroclastic texture with coarse-grained porphyroclasts (ca. 0.2–5 mm) and finer grains (<200 μm) (Figs. 2, 3).

Coarse grains show up to 3 distinct zones: a chemically distinct core (CIa, dark area in Fig. 2), a chemically distinct inner rim (CIb, Fig. 2), and an outer rim that exhibits both distinct chemistry and intercrystalline deformation defined by several low-angle boundaries (CII, Fig. 2a, b). The compositional zonation of coarse-grained chromites from zone CIa to CIb is clearly associated with euhedral-shaped cores showing {111} and {100} facet planes (Fig. 2d). Silicate inclusions (chlorite and antigorite; ca. 10–50 μm) are present in the rims of large grains (Fig. 2a). The smaller size fractions of the coarse-grained chromites often exhibit zones CIb and CII with crystal-plastic deformation features such as subgrain boundaries (Fig. 3b) and progressive crystal bending with a cumulative misorientation of ≤10° (Fig. 3d, e). While the chemically distinct CIb and CII are commonly observed (Fig. 4), zone CIa is only rarely preserved. In contrast, zone CII is always present at the rim of the porphyroclast and exhibits significant crystallographic orientation changes within the grains in all studied cases, i.e. subgrain boundaries that accommodate progressive lattice bending (Figs. 3b, d, e and 4f, g).

Fine-grained chromite grains are spatially closely associated with the coarse grains and are dominantly nearly inclusion-free. These chromite grains display two distinctly different types referred to as F1

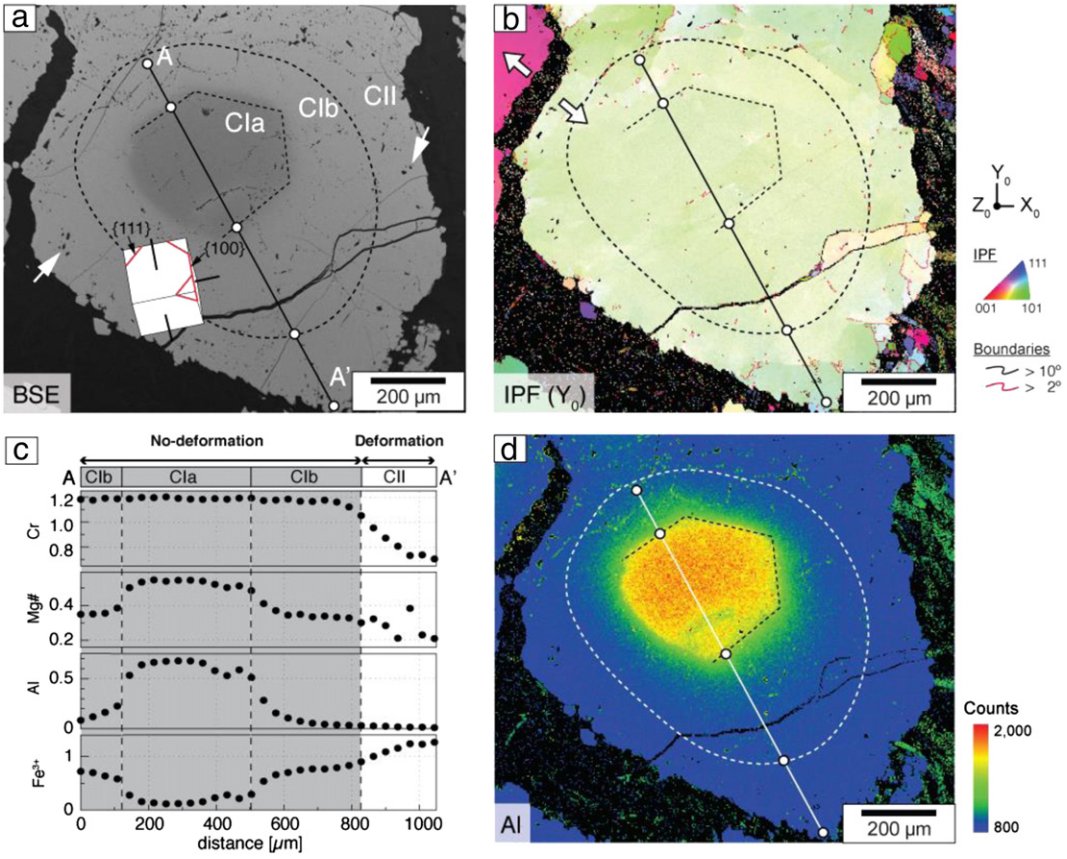

Fig. 2. Characteristics of coarse-grained zoned chromite. (a) Back-scattered electron image showing clear chemical zonation. There are 3 distinct zones: a chemically distinct core (CIa), a chemically distinct outer core (CIb) and an outer rim that exhibits both distinct chemistry and intercrystalline deformation defined by several low-angle boundaries (CII). Red lines in small white cubic represent {111} and {100} low index planes corresponding to euhedral-shaped cores (CIa). White arrows represent the silicate inclusions. (b) EBSD map showing crystal orientation changes relative to the Y_0 direction of the sample reference frame. Step size of the map is 3 μm. Thick white arrows represent directions of movement of late brittle fractures. Note the presence of subgrain boundaries dominantly at outer parts of the chromite grain. (c) Chemical profile A–A′ in (a) for Cr, Mg#, Al and Fe^{3+}. (d) EDS map of Al contents.

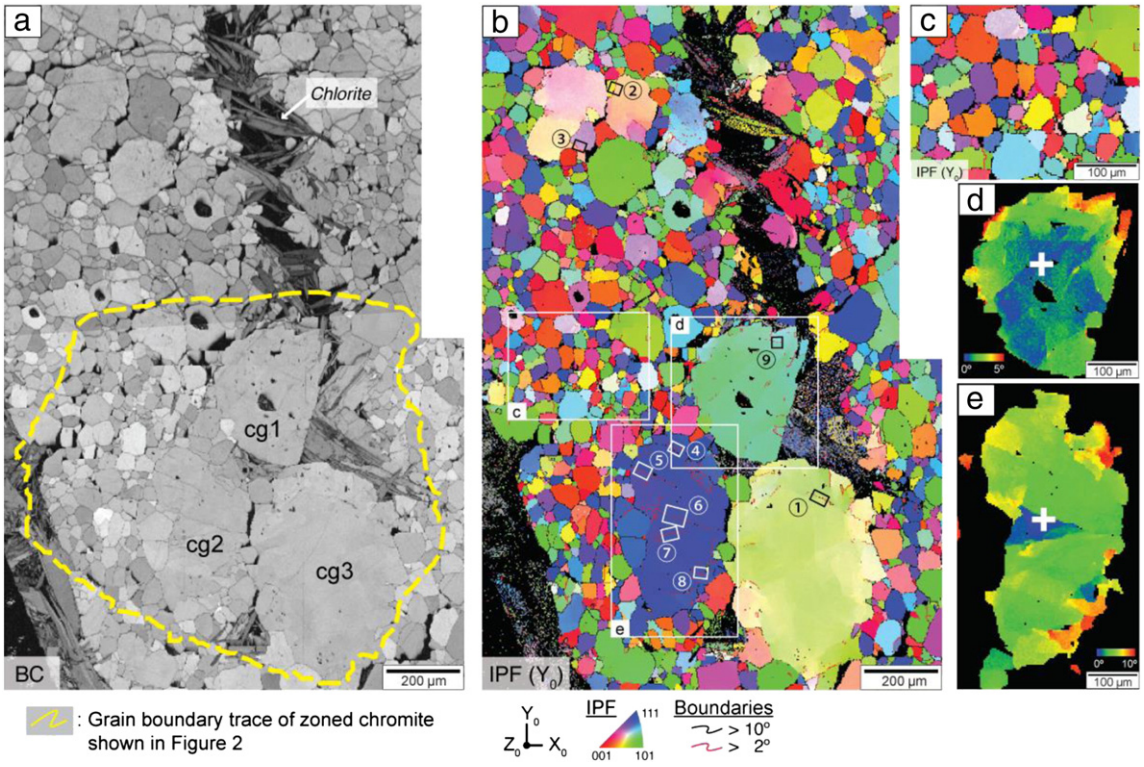

Fig. 3. Microstructure of coarse-grained chromite porphyroclasts and fine-grained chromite grains as revealed by EBSD analysis. (a) Orientation contrast map showing in different gray scale changes in crystallographic orientations. Dark areas are grain boundaries, holes and fractures. Dark elongate features represent undeformed chlorite grains. A dotted yellow line represents the grain boundary trace of the coarse-grained zoned chromite in Fig. 2. (b, c) EBSD maps where colors show different orientations. Step size of the map is 3 μm. (b) White rectangles mark the location of detail maps (c) to (e). Note that black and white small rectangles with enclosed numbers mark the area used for the subgrain boundary analysis in Fig. 7. (c) Close-up EBSD map of fine grains. (d, e) EBSD map of coarse grains showing change of orientation from a reference orientation (white cross) by a maximum misorientation of 5° (d) and 10° (e), respectively. Step size of the map is 3 μm.

and F2 in the following description. Type F1 grains show an average misorientation of ≤1° within an individual grain (Fig. 4a), no subgrain boundaries (Fig. 4b, d, f), and an equilibrated equigranular microstructure (Fig. 3c). Straight to slightly curved grain boundaries define a polygonal grain-boundary network with well-developed 120° triple and quadruple junctions.

Type F2 grains show significant local orientation changes within individual grains exhibiting abundant low-angle boundaries and lattice distortions in the order of 1–8° (Fig. 4a). F2 grains have curved to lobate grain boundaries, which define anhedral grain shapes (Fig. 4b–g). Misorientation profiles across low- to high-angle boundaries show a stepwise orientation change (Fig. 4h). The size of F2 grains is the range of the subgrain size seen within the rim areas of porphyroclasts (Fig. 4i).

In summary, F1 grains chromites are well-equilibrated and dominantly undeformed, whereas F2 grains show deformation-induced crystallographic orientation changes. F1 grains are slightly smaller (range: 13.1–179.6 μm; average: 32.3 ± 18.2 μm) than F2 grains (range: 13.7–199.3 μm; average: 53.8 ± 35.8 μm).

Euhedral grains of clinochlore are present between chromite grains (Fig. 3a). Furthermore, late fractures along grain boundaries are observed (Fig. 2b); these show no mineral infill.

Orientation data from all chromite grains analyzed display near-random to very weak patterns of bulk crystallographic preferred orientation (CPO) with numerous orientation maxima at <100>, <110>, and <111> (Fig. 5a). To characterize CPOs, we determined the fabric strength and distribution density of the principal crystallographic axes by calculating the *J* index of the orientation distribution function (ODF), simply called pfJ (J index of pole figures) (e.g., Bunge, 1982; Mainprice and Silver, 1993). Type F2 grains exhibit a relatively strong CPO (pfJ of <100>, <110>, and <111> is 1.05, 1.02, and 1.04, respectively), which is distinct from that of the coarse grains and F1 grains (pfJ of <100>, <110>, and <111> is 1.01, 1.00, and 1.01, respectively) (Fig. 5b). The number of measurements may cause this small difference in pfJ strength; more than 1000 F1 grains were measured, whereas 218 F2 grains were measured. At a local scale, F2 grains exhibit crystallographic affinity to the adjacent porphyroclast (Fig. 4i). In contrast, type F1 grains are distributed more randomly and show a large variation in orientations with no direct correlation to that of the adjacent porphyroclast (Fig. 5c). Misorientation analysis of low-angle boundaries shows that rotation axes are dominantly <112> with {111}<110> and {110}<112> slip system but also rotations around <100> and <110> also occur (Fig. 6).

4.2. Mineral chemistry

Major-element analyses on Golyamo Kamenyane chromites including coarse grains (Zoned, CIa, CIb, CII) and fine grains (F1, F2) show a distinct relationship between deformation and chemical environment (Supplementary Table 1, Fig. 4). In general, the Cr_2O_3 and MgO contents range between 23.8–47.8 wt.% and 3.73–11.4 wt.%, respectively (Supplementary Table 1). TiO_2 shows a maximum value of 0.20 wt.%. These general compositions are consistent with those of previously analyzed Golyamo Kamenyane chromitites (Colás et al., 2014; Gervilla et al., 2012). Chromites have Mg# values of 0.21–0.55, Cr# values of 0.64–0.99, and Fe^{3+} values of 0.21–0.55 (Supplementary Table 1, Figs. 2c, 7). Coarse-grained type CIa and CIb domains (commonly undeformed area) have Fe^{3+} values of 0.25–0.29, which are mostly lower than those of CII (deformed area) domains (0.28–0.36) (Supplementary Table 1, Fig. 7a). Among the fine-grained chromites, F1 grains have more homogeneous compositions than F2. Cr and Fe^{3+} values range between 0.69–0.72 and 1.25–1.27, and between 0.69–0.76 and 1.21–1.28 for F1 and F2, respectively (Supplementary Table 1, Fig. 7a, c). This near-homogeneous chemical signal in the fine-grained chromites is well

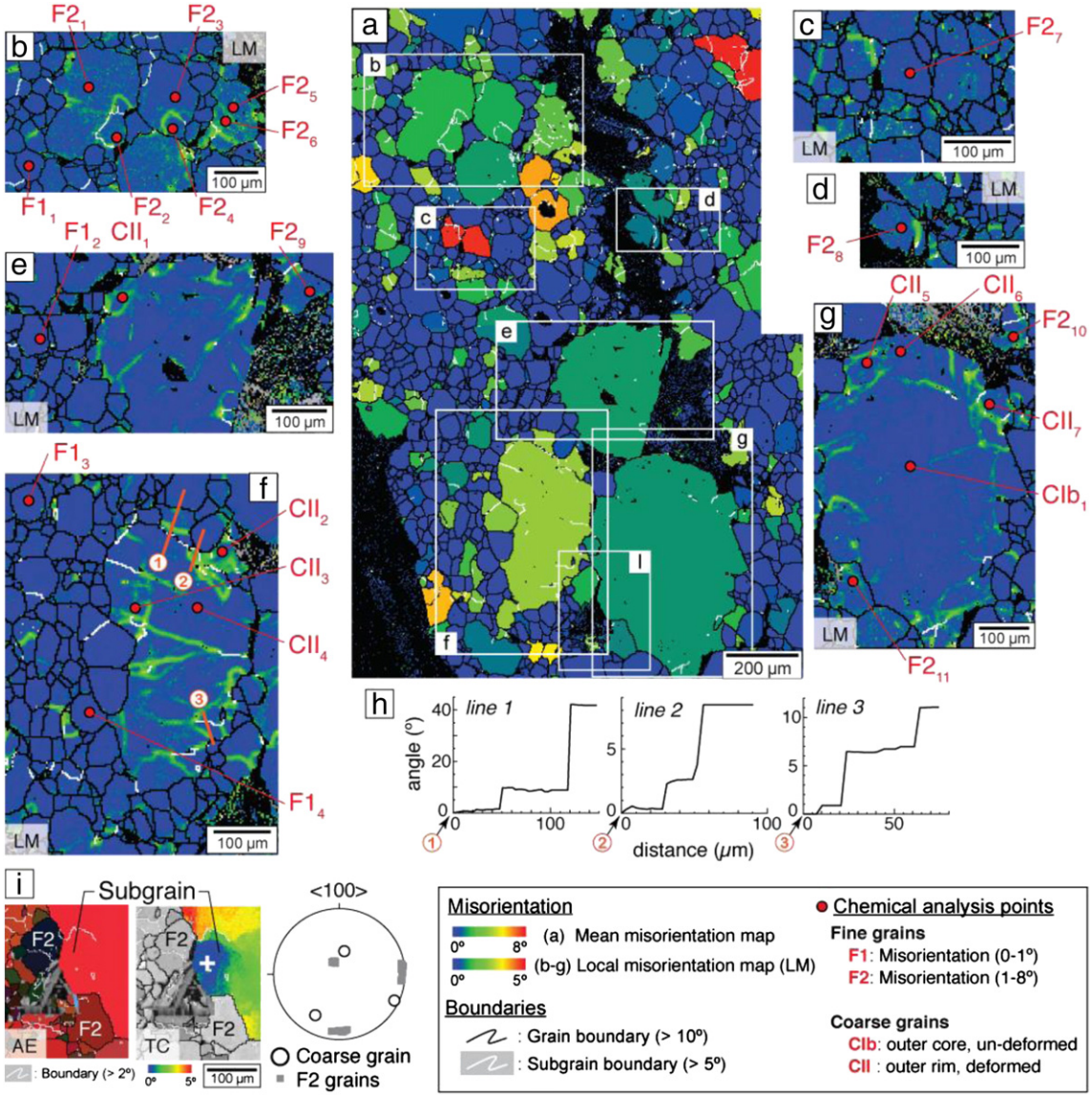

Fig. 4. Orientation relationships as well as chemical composition of chromite porphyroclasts and adjacent fine grains. Step size of the map is 3 μm. (a) Color coded EBSD map depicting the mean misorientation per grain (mean misorientation map). (b–g) EBSD maps showing local misorientations (LM) to identify crystal bending and subgrain boundaries below 5°. Fine grain types F1 and F2 are depicted (see text for definition). Chemical compositions at each red point are shown in Supplementary Table 1 and categorized according to fine grain type (F1, F2) and coarse grain domain (CII, CIb; see text for details). (h) Misorientation profiles along the solid orange lines with enclosed numbers (lines 1, 2, and 3) in (f). (i) EBSD map showing all euler angles (left) and cumulative orientation map showing maximum misorientation of 5° relative to crystal orientation at the position marked by a white cross (middle). Crystallographic preferred orientation (CPO) data of given chromites (right). Data are presented on lower-hemisphere equal-area pole figure, and <100> axis is presented. Note that F2 grains are in a size range similar to that of subgrains in coarse grains, and they show distinct crystallographic affinity.

illustrated by the EDS map (Fig. 7d), which shows progressive chemical modification from zoned coarse grains to fine grains.

5. Discussion

5.1. Microstructures in highly strained chromitite: underlying physicochemical processes

The microstructures observed in the studied chromites are consistent with recrystallization microstructures reported from many geological materials (e.g. Drury and Urai, 1990; Passchier and Trouw, 2005). The porphyroclastic texture consisting of coarse-grained chromite porphyroclasts (ca. 0.2–5 mm) and fine-grained chromite neoblasts (<200 μm) (Fig. 3a) is typical of deformation involving dominantly ductile, crystal plastic deformation (Passchier and Trouw, 2005). Within large porphyroclasts, the igneous chemical signature is preserved in terms of major elements (i.e. CIa). This chemical zoning with clearly distinguishable euhedral-shaped cores corresponding to the {111} and {100} facet planes (Fig. 2a) suggests that the grains initially grew with perfect facets during crystallization. Such igneous growth patterns are analogous to the well-documented igneous zonation in igneous feldspars and pyroxenes (e.g., Holness and Watt, 2001). The initial CIa cores are high in Mg# and Al, while the second domain (CIb) exhibits chemical equilibration in an environment with higher availability of Fe^{3+} (Fig. 2c) (Colás et al., 2014). Domains CIa and CIb existed before the deformation event, which is studied here in detail. In contrast to CIa and CIb, the chemically distinct zone CII (higher of Fe^{3+} and lower of Mg# and Cr) (Fig. 2c) is spatially coupled with intracrystalline deformation, suggesting that local chemical re-equilibration accompanied crystal-plastic deformation of the outer zone during the retrograde

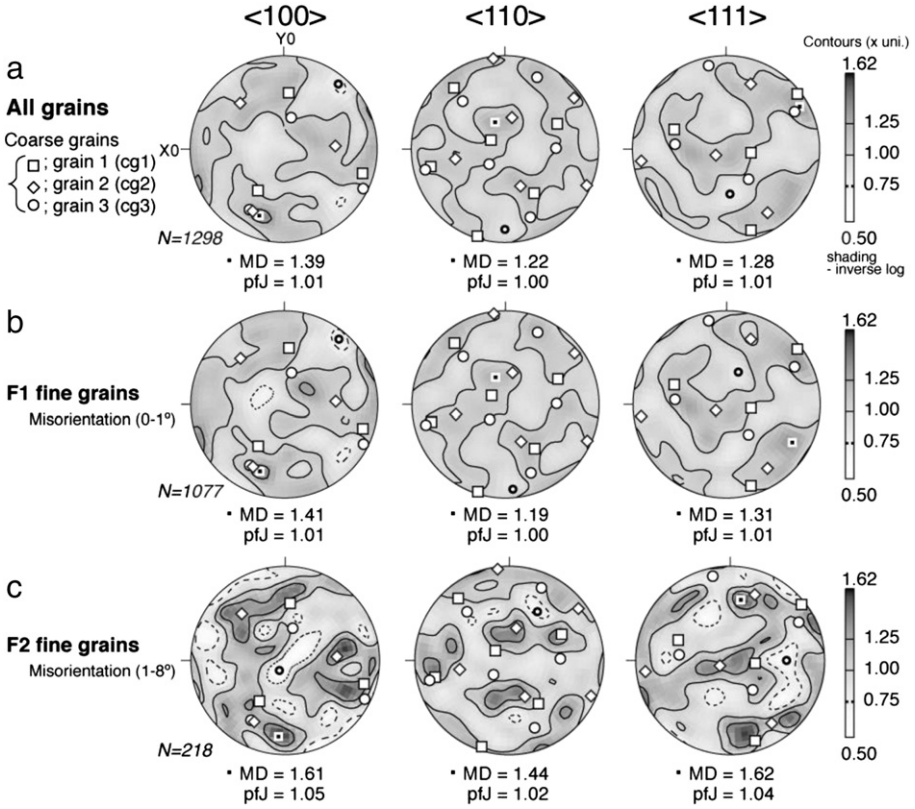

Fig. 5. Crystallographic preferred orientation (CPO) data of chromite in this study. Data are one point per grain data, smoothed with a Gaussian fit of 8.5° half-width and presented on lower-hemisphere equal-area pole figure. pfJ is an index of pole figure intensity, and MD is the maximum pole figure density in times uniform distribution. For axes, <100>, <110>, and <111> are presented. (a) All grains. (b) Nucleated grains (F1) with internal misorientation below 1°. (c) Recrystallized grains (F2) with internal misorientation between 1 to 8°. White diamond, square, and circle represent CPO of the 3 coarse grains depicted in Fig. 2 (cg1, cg2, cg3).

tectonometamorphic event. This third domain CII shows a significant non-concentric in chemical zoning, which suggests that growth did not occur in a melt but that grains where chemically modified have crystallization. We suggest that the observed chemical change is due to the replacement of the original chromite by one of the $(Fe^{2+}, Mg)(Fe^{3+}, Cr)_2O_4$ compositions as the chemical environment changed due to the influx of external fluids during deformation. Such fluid-mediated replacement reactions (e.g. Putnis, 2009) may also explain the observed inclusion of hydrous phases. Observations supporting a replacement reaction are:

(i) Relatively sharp boundary between CIb and CII chemical profiles which cannot be explained by diffusion alone
(ii) Presence of fine-grained hydrous phases as inclusions
(iii) Epitaxial relationship between the CIb and CII chromite (Fig. 2d).

If such a replacement reaction occurs during deformation, asymmetric replacement is expected to occur along with formation of subgrain boundaries and crystal bending. The fact that only the rims of large coarse grains have been subject to crystal-plastic deformation is consistent with the fact that stress magnitudes are greatest at grain interfaces (e.g. Hull and Rimmer, 1959; Montagnat et al., 2011; Svahnberg and Piazolo, 2012, and reference therein).

During high-strain deformation, strain is commonly accommodated by grain-size reduction. Grain network modification in deforming rocks may be driven by chemical reactions (chemically-induced grain boundary migration), by reduction of stored energy associated with defects (static or primary recrystallization), or by reduction of boundary energy (grain growth; Drury and Urai, 1990; Urai et al., 1986). Three main deformation mechanisms have been proposed for grain size reduction: 1) subgrain rotation recrystallization (SGR) (e.g., Drury and Urai, 1990; Yund and Tullis, 1991), 2) heterogeneous nucleation and growth of new grains and 3) bulging (BLG) recrystallization facilitated by grain boundary migration (e.g. Drury and Urai, 1990).

During SGR, a subgrain undergoes recrystallization by rotation if all of its low-angle boundaries evolve from low-angle boundaries to high-angle boundaries as dislocations are continuously added to subgrain boundaries (e.g., Drury and Urai, 1990; Halfpenny et al., 2006 and references therein). SGR recrystallization should theoretically produce new grains with boundary angles only slightly higher than 10° (Trimby et al., 1998) without significant compositional change and similar in size to subgrains within the host. Furthermore, such subgrains will inherit internal deformation features similar to those of the host (e.g., Kruse et al., 2001).

Heterogeneous nucleation and growth of relatively strain- and dislocation-free new grains (Doherty et al., 1997) develop in highly strained areas within the host grain. These are commonly close to the rim of the grains. This produces grains whose composition reflects the thermodynamically favorable composition at the time of nucleation and growth. Therefore, the chemistry of such grains is extremely useful in pinpointing the physicochemical conditions during their formation and growth (Kruse and Stünitz, 1999).

At low temperature, where grain-boundary migration may be local, a grain boundary may bulge into the crystal with high dislocation density and form new, independent small crystals (e.g., Drury and Urai, 1990; Stipp et al., 2002). This process is known as BLG recrystallization, and occurs mostly along the boundaries of old grains at triple junctions. The bulges may separate from the host grain to form small independent new grains by formation of subgrain boundaries, which evolve into grain boundaries (Urai et al., 1986), or by grain-boundary migration (Stipp et al., 2002).

In this study, small grains are almost inclusion-free in comparison to coarse grains (Fig. 3a), which have silicate inclusions (chlorite and

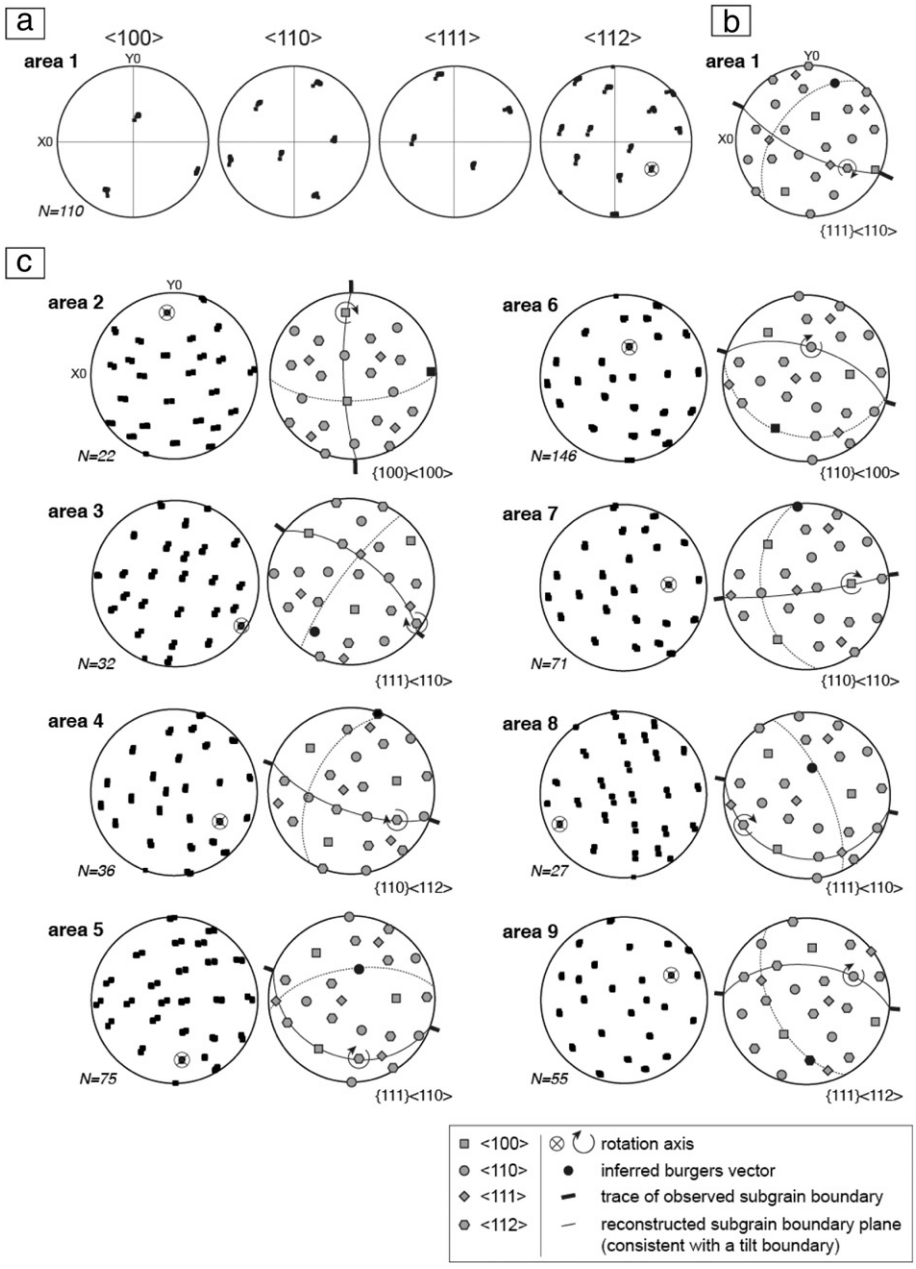

Fig. 6. Boundary trace analysis to determine the active slip system consistent with orientation changes across subgrain boundaries for 9 selected areas. Data are presented on lower-hemisphere equal-area pole figure. N is the number of data points. For each area, the orientation of individual axes is shown as well as the interpretation in terms of rotation axis, inferred Burgers vector position and the activated slip systems in terms of slip plane and slip direction. (a) Orientation data from analyzed area 1 (Fig. 4a). (b) Schematic representations of CPOs shown in (a) in a pole figure. (c) Orientation data and data interpretation for areas 2–9 (cf. Fig. 4 for location of analyzed areas).

antigorite) mainly in their rim (Fig. 2a). This implies that fine grains recrystallized under conditions in which there was no crystallization of silicates. Recrystallization processes in chromite have been described only from a few occurrences. Similar inclusion-free recrystallized chromite grains showing a change in chemistry have been described from the Fiskenaesset deposit of West Greenland (Ghisler, 1976), the Oman ophiolite complex (Christiansen, 1985), and the Sittampundi anorthosites complex in India (Ghosh and Konar, 2012). Ghisler (1976) presented evidence for recrystallization of chromite in the most deformed parts of a pre-orogenic stratiform complex. The often irregular recrystallized grains are devoid of silicate inclusions and show a change in chemistry from the magmatic chromite. The Oman samples also show a progressive change from euhedral chromite grains with abundant inclusions to grains with few inclusions (Christiansen, 1985).

The two types of recrystallized, small grains, F1 and F2, are consistent with heterogeneous nucleation and formation due to subgrain rotation recrystallization, respectively. Crystallographic and grain relationships show that F2 grains are in the same size range as the subgrains observed in coarse chromites (Fig. 4i). At the same time, the F2 grains in the vicinity of a large chromite grain show distinct crystallographic affinity, consistent with progressive rotation of a subgrain to form a grain during ongoing deformation (Fig. 4i). F1 grains, in contrast, show distinctly different orientations to adjacent grains (Fig. 5b).

The retrograde P–T exhumation path defined by the thermodynamic and chemical modeling suggests that these fine-grained chromites were produced when the chromitites reacted with oxidizing fluids during retrograde metamorphism (Colás et al., 2014; Gervilla et al., 2012). This allowed the enrichment of Fe^{3+} (and at lesser extent Fe^{2+}) in the rims of coarse grains and the formation of fine-grained Fe^{3+}-rich F1

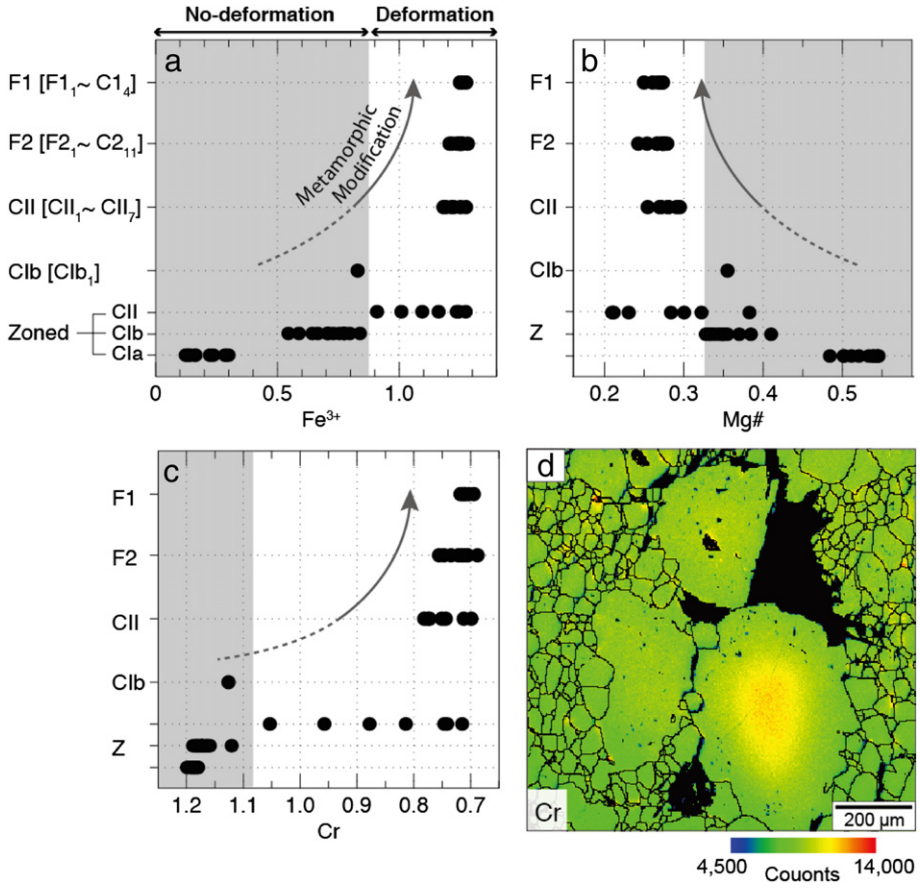

Fig. 7. Differences in chemical composition of different coarse-grained chromite domains (CIa, CIb and CII) and fine chromite grain types (F1 and F2) shown in Figs. 3 and 4. (a–c) Fe^{3+}, Mg#, and Cr data, note that coarse grains have a general Cr-rich, Fe^{3+}-poor composition relative to the fine grains. (d) EDS map of Cr contents of the overview map shown in Figs. 3 and 4.

chromite (i.e., ferrian chromite). F1 chromite was less affected by chemical re-equilibration, and the original igneous signature is cryptically preserved. Local chemical re-equilibration occurred additionally at grain boundaries and subgrain boundaries, where pipe diffusion in the deformed crystal lattice facilitates accelerated local chemical equilibration (e.g. Piazolo et al., 2012; Reddy et al., 2007).

The relationships between microstructure and chemical evolution are demonstrated in other rocks, as found by Kruse and Stünitz (1999) for mylonites in anorthositic to gabbroic rocks. They showed that the compositional difference between porphyroclasts and recrystallized grains in hornblende is not due to diffusional exchange after recrystallization, but probably is due to heterogeneous nucleation and growth of compositionally different hornblende. It is also inferred that heterogeneous nucleation of plagioclase, hornblende and pyroxenes due to chemical disequilibrium produces mixtures of phases (Svahnberg and Piazolo, 2012).

The role of deformation mechanism in the effectiveness of local chemical re-equilibration becomes clear when examining the differences in chemical composition between coarse-grained (including zoned- chromite) and fine-grained chromites (Fig. 7a–c). These data clearly show the continuous variation of chemical composition as a function of microstructure; the nucleated grains (F1) have higher Fe^{3+} and Cr (atomic) values and lower Mg#, whereas F2 grains have intermediate values, and coarse grains have variable compositions with lower Fe^{3+} and Cr and higher Mg# (CIa, CIb, CII) (Fig. 7a–c). The close physicochemical link between chromite composition and its deformation features (Fig. 7a–c) suggests that compositionally homogeneous fine-grained chromites (Fig. 7d) were formed during the deformation event. Thus, subgrain rotation and chemical modification formed type F2 chromite, whereas type F1 chromite grains were produced by nucleation and the growth of new grains in the presence of oxidizing fluids. Overall, deformation in different chemical environments produced two different kinds of fine-grained, chromite grains with a narrow range in compositions and chemical homogenization by reaction with oxidizing fluids and the nucleation and growth of new grains through metamorphic re-equilibration.

As described above, our observations show a continuous physicochemical process; and microstructural evolution due to crystal-plastic deformation involved the formation and migration of dislocations, subgrain rotation recrystallization, and nucleation. All of the observed microstructural features, such as intracrystalline deformation defined by low-angle boundaries, and dynamic recrystallization of chromite by subgrain rotation and heterogeneous nucleation, are typical of deformation in dislocation-creep regimes (Passchier and Trouw, 2005; Urai et al., 1986). Thus, deformation was accommodated by dislocation creep but not by diffusion creep. Experimental studies of magnetite, which is a non-silicate with a spinel structure like chromite, have revealed that magnetite can undergo intracrystalline deformation by dislocation creep (Hennig-Michaeli and Siemes, 1982; Müller and Siemes, 1972). Recent experiments on the deformation of magnetite (Till and Moskowitz, 2013) present new flow laws and give a stress exponent value around 3, and hence we argue that the flow character is non-Newtonian, power-law creep with a stress exponent of around 3. Dislocation creep previously was not thought to be a dominant mechanism; instead, diffusional creep, which normally does not result in a strong crystallographic fabric (Wheeler, 2009) and intracrystalline deformation features, was considered the principal mechanism in the deformation of chromites (Ozawa, 1989). However, our observations show that dislocation creep plays an important role in chromite deformation at amphibolite facies conditions.

5.2. Chromite fabric and slip system activation

During progressive crystal-plastic deformation, grain orientations tend to produce distinct patterns, because deformation is mainly accommodated by one or a few most favorable slip systems, and it follows that the deformed mineral acquires a preferred orientation (Law et al., 1990). However, the representation of a CPO for chromite in natural rock samples is complex because of its cubic symmetry. Also, chromites may be subsequently recrystallized, with nucleation and growth, which would make the CPO pattern weaker.

Chromite has a cubic symmetry with face-centered-cubic (*fcc*) packing and the space group *Fd3m*. Although the deformation mechanisms and CPOs of chromite are still poorly understood, we can compare data with experimental results on the deformation of *fcc* metals. The chromite examined in this study does not have a strong CPO pattern (pfJ < 2.0), but there are two weak girdle concentrations in <111>, a pattern that has been observed in cold-rolled aluminum (a *fcc* metal) (Grewen and Huber, 1978). This weak CPO might suggest that deformation was insufficient to realign the chromite into a strong preferred orientation (pfJ > 2.0).

The EBSD maps of our samples suggest that crystal-plastic deformation has generated chromite subgrains and new grains in response to recrystallization processes (Fig. 4a). The dislocations may be either spatially-distributed or arranged along distinct subgrain boundaries. In the latter case, dislocations of a particular geometry will form dislocation arrays with a particular rotation axis and orientation within the crystal. To infer an active slip system, it is possible to use the orientation of the misorientation axis as defined by dispersions and measured orientation of the subgrain boundaries to define the most likely type of dislocations involved, the activated slip systems and the type (tilt or twist boundary) of the analyzed subgrain boundary (Piazolo et al., 2008; Prior et al., 2002).

Our samples contain some well-defined low-angle subgrain boundaries (2–10° misorientation on either side) (Fig. 3b). Using the boundary trace technique described above, the analysis of area 1 (small white rectangle with enclosed number 1 in Fig. 3b) is presented in Fig. 6(a, b). The trace of the subgrain boundary does not lie in a plane perpendicular to the misorientation axis (Fig. 6b) as determined by the dispersion paths depicted in the pole figure (Fig. 6a). Thus, we can eliminate a twist-boundary model for this subgrain boundary. A steep plane that contains the subgrain-boundary trace and the determined misorientation axis <112> (Fig. 6b) is the probable subgrain boundary plane, in this case {110}. This geometry is consistent with the subgrain boundary comprising an array of edge dislocations lying in the {110} plane. The misorientation axis can be explained by the activation of {110}<111> or slip system (Fig. 6b).

A similar analysis can be made of other areas (areas 2–9, Figs. 3b, 6c). For these, the misorientation axis lies in the plane that is consistent with the trace of the observed boundaries, so the subgrain boundaries are consistent with a tilt boundary. The rotation axes are in the plane that forms the trace of the subgrain boundary. Consequently, active slip systems are {111}<110> (areas 3, 5 and 8), {110}<112> (area 4), {110}<100> (area 6), {110}<110> (area 7), {100}<100> (area 2), and {111}<112> (area 9) with the dominant slip system {111}<100>.

Our results are consistent with previous deformation studies on *fcc* metal where it was found that in such materials the {111}<110> slip is dominantly activated (Humphreys and Fatherly, 2004). Other slip systems sometimes operate due to stress and strain incompatibilities (e.g. Montagnat et al., 2011).

5.3. Microstructural evolution of deformed chromitite at mid-crustal conditions

The spatial correlation between crystallographic and chemical relationships observed here allows us to develop a model of microstructural evolution during deformation of chromitites at mid-crustal levels (~1.0 GPa and 500–700 °C; Gervilla et al., 2012) (Fig. 8). The chromitites in our samples were affected by amphibole-facies tectonometamorphism in the presence of oxidizing Fe^{3+}-rich fluids (Colás et al., 2014; Gervilla et al., 2012), and these re-equilibrated chromites have clear evidence of crystal-plastic deformation. According to above discussion, we interpret the deformation history as Stage I: Pre-deformational initial chromites with nucleation and growth-related chemical zoning (Fig. 8a). These large chromites are undeformed, and different timing of nucleation produced variation in size and chemical signature. Stage II (IIa and IIb): Syn-deformational chemical modification due to metamorphism. During Stage IIa, infiltration of oxidizing fluids and crystal-plastic deformation of coarse grains in the dislocation-creep regime occurred at the same time. Coarse grains were recrystallized to fine grains by subgrain rotation or nucleation (Fig. 8b; Stage IIa). Crystal-plastic deformation produced dynamic porosity (e.g., Behrmann, 1985; Billia et al., 2013; Fusseis et al., 2009; Menegon et al., 2015; Rybacki et al., 2008; Timms et al., 2012)

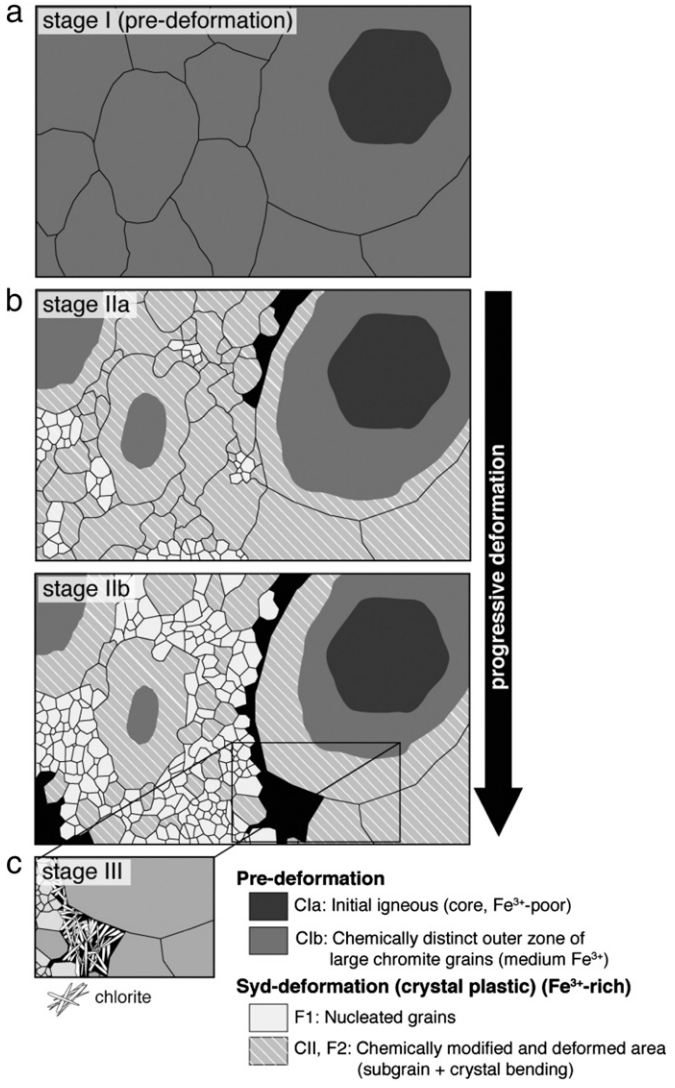

Fig. 8. Schematic model of the evolution of the chromite sample investigated. (a) Stage I: Pre-deformation. Initial chromitites with chemically zoned coarse-grained chromite. (b) Stage II (IIa and IIb): Syn-deformation. Stage IIa: Contemporaneous fluid percolation and deformation, resulting in modified chemical composition crystal-plastic deformation of coarse-grained chromite which forms subgrains, develop crystal bending and related chemical modification. Further deformation causes nucleation of chemically distinct chromite grains by heterogeneous nucleation (F1) and by subgrain rotation recrystallization (F2). Stage IIb: Progressive deformation produced a large number of fine grains (F1 and F2). (c) Stages III: Precipitation and growth of chlorite.

and at the same time, fluid influx accelerated recrystallization processes aiding strain weakening and thus strain localization. Consequently, deformation-induced fluid influx aided further strain localization and shear zone formation. During the progressive deformation, some recrystallized grains continued to deform internally. Continuous chemical modification produces chemical homogenization (Fig. 8b; Stage IIb). During the crystal-plastic deformation in Stage II, several slip systems were activated. Stage III: After the main deformation event, chlorite grains grew in late fractures along grain boundaries formed at lower temperatures, possibly during emplacement to the surface resulting in pull-apart microstructures (Figs. 3a, 8c).

The fact that the studied chromites are the most chemically modified and deformed in the Golyamo Kamenyane (Colás et al., 2014) indicates that fluid flux and shear-zone formation are closely linked, where fluid aided recrystallization, strain localization and local chemical re-equilibration. Overall, the main deformation occurred in the dislocation creep regime in localized shear zones within the chromitite body. It was accompanied by the introduction of oxidizing fluids at temperatures below 600 °C within a chemically distinct environment in an open-system metamorphic environment resulting in chemical homogenization of chromite during metamorphic re-equilibration.

6. Implications and conclusions

The identification and characterization of deformation mechanisms in chromite-rich zones play an important role in understanding the rheological and chemical behavior of chromitite in the global convection cycle, but new technology and methodologies have only recently made this goal attainable.

In this study, we have utilized EBSD analysis allowing in depth investigation of deformation features, combined with compositional data to explore the effect of deformation and chromite chemistry. Our results suggest that the microstructures in the chromite grains of the metamorphosed chromitites of Golyamo Kamenyane were produced by fluid-present crystal-plastic deformation. This process took place during metamorphic re-equilibration when oxidizing fluids were introduced into the system, precipitating ferrian chromite. The chromites show porphyroclastic texture with coarse-grained porphyroclasts (ca. 0.2–5 mm) and fine-grained neoblasts (<200 μm). Coarse-grained chromites preserve both igneous and metamorphic signatures in terms of major elements, whereas fine-grained chromites produced by plastic deformation have chemical compositions imposed during metamorphism. The microstructures such as intracrystalline deformation defined by continuous lattice bending and low-angle boundaries, small recrystallized chromite grains and remnant large chromite porphyroclasts indicate that dislocation creep involving intracrystalline slip and subgrain rotation and nucleation recrystallization, accommodated chromite deformation at mid-crustal conditions.

Chromitite is commonly assumed to be resistant to fluid-related processes, however, this study illustrates for the first time a clear interaction between deformation history and the chemical properties of chromite. This interaction occurred during fluid-present deformation where chromite deformed in the dislocation-creep regime in a chemically distinct system. We suggest that during deformation, stress-induced nucleation and subgrain rotation induced a deformation-enhanced chemical modification. This study highlights the fact that in-depth studies of both deformation and chemical features in chromite may lead to refined and/or new interpretation of chromite characteristics. The recognition of the close link between chemistry and deformation offers new avenues for the utilization of chromite characteristics in petrological and tectonic studies, which has a potential to use as a tracer of global element recycling from mantle to crust.

Supplementary data to this article can be found online at http://dx.doi.org/10.1016/j.lithos.2015.04.020.

Acknowledgments

Pole figures were plotted using the interactive programs developed by D. Mainprice of Université Montpelier II, France. The analytical data were obtained using instrumentation funded by DEST Systemic Infrastructure Grants, ARC LIEF, NCRIS, industry partners and Macquarie University. This manuscript was greatly improved by careful reviews of L.F.G. Morales and N. Timms. SP acknowledges funding from the Australian Research Council (DP120102060, FT1101100070). This is contribution 622 from the ARC Centre of Excellence for Core to Crust Fluid Systems (http://www.ccfs.mq.edu.au) and 1007 in the GEMOC Key Centre (http://www.gemoc.mq.edu.au).

References

Arai, S., 1992. Chemistry of chromium spinel in volcanic rocks as a potential guide to magma history. Mining Magazine 56, 173–184.
Arai, S., 1997. Control of wall-rock composition on the formation of podiform chromitites as a result of magma/peridotite interaction. Resource Geology 47, 177–187.
Arai, S., 2010. Possible recycled origin for ultrahigh-pressure chromitites in ophiolites. Journal of Mineralogical and Petrological Sciences 105, 280–285.
Arai, S., 2013. Conversion of low-pressure chromitites to ultrahigh-pressure chromitites by deep recycling: a good inference. Earth and Planetary Science Letters 379, 81–87.
Arai, S., Abe, N., 1995. Reaction of orthopyroxene in peridotite xenoliths with alkali-basalt melt and its implication for genesis of alpine-type chromitites. American Mineralogist 80, 1041–1047.
Arai, S., Yurimoto, H., 1994. Podiform chromites of the Tari–Misaka ultramafic complex, southwestern Japan, as mantle–melt interaction products. Economic Geology 89, 1279–1288.
Barnes, S.J., Roeder, P.L., 2001. The range of spinel compositions in terrestrial mafic and ultramafic rocks. Journal of Petrology 42, 2279–2302.
Barrie, C.D., Boyle, A.P., Cox, S.F., Prior, D.J., 2008. Slip systems and critical resolved shear stress in pyrite: an electron backscatter diffraction (EBSD) investigation. Mineralogical Magazine 72 (6), 1181–1199.
Beane, R.J., Field, C.K., 2007. Kyanite deformation in whiteschist of the ultrahigh-pressure metamorphic Kokchetav Massif, Kazakhstan. Journal of Metamorphic Geology 25, 117–128.
Behrmann, J.H., 1985. Crystal plasticity and super plasticity in quartzite: a natural example. Tectonophysics 115, 101–129.
Bestmann, M., Prior, D.J., 2003. Intragranular dynamic recrystallization in naturally deformed calcite marble: diffusion accommodated grain boundary sliding as a result or subgrain rotation recrystallization. Journal of Structural Geology 25, 1597–1613.
Billia, M.A., Timms, N.E., Toy, V.G., Hart, R.D., Prior, D.J., 2013. Grain boundary dissolution porosity in quartzofeldspathic ultramylonites: implications for permeability enhancement and weakening of mid-crustal shear zones. Journal of Structural Geology 53, 2–14.
Bonev, N., 2006. Cenozoic tectonic evolution of the Eastern Rhodope massif (Bulgaria): basement structure and kinematics of syn- to post-collisional extensional deformation. In: Dilek, Y., Pauides, S. (Eds.), Mediterranean Region and Asia. Geol. Soc. Am. Spec. Paper 49, pp. 211–235.
Borthwick, V.E., Piazolo, S., 2010. Complex temperature dependent behaviour revealed by in-situ heating experiments on single crystals of deformed halite: new ways to recognize and evaluate annealing in geological materials. Journal of Structural Geology 32, 982–996.
Bunge, H.J., 1982. Texture Analysis in Materials Sciences. Butterworth, London.
Büttner, S.H., 2005. Deformation-controlled cation diffusion in compositionally zoned tourmaline. Mining Magazine 69 (4), 471–489.
Christiansen, F.G., 1985. Deformation fabric and microstructures in ophiolitic chromitites and host ultramafics, Sultanate of Oman. Geologische Rundschau 74, 61–76.
Christiansen, F.G., 1986. Deformation of chromite: S.E.M. investigations. Tectonophysics 121, 175–196.
Colás, V., González-Jiménez, J.M., Griffin, W.L., Fanlo, I., Gervilla, F., O'Reilly, S.Y., Pearson, N.J., Kerestedjian, T., Proenza, J.A., 2014. Fingerprints of metamorphism in chromite: new insights from minor and trace elements. Chemical Geology 389, 137–152.
Doherty, R.D., Hughes, D.A., Humphreys, F.J., Jonas, J.J., Juul Jensen, D., Kassner, M.E., King, W.E., McNelley, T.R., McQueen, H.J., Rollet, A.D., 1997. Current issues in recrystallization: a review. Materials Science and Engineering A238, 219–274.
Drury, M.R., Urai, J.L., 1990. Deformation-related recrystallization processes. Tectonophysics 172, 35–253.
Erickson, T.M., Pearce, M.A., Taylor, R.J.M., Timms, N.E., Clarck, C., Reddy, S.M., Buick, I.S., 2015. Deformed monazite yields high-temperature tectonic ages. Geology http://dx.doi.org/10.1130/G36533.1.
Frost, H.J., Ashby, M.F., 1982. Deformation-mechanism Maps. The Plasticity and Creep of Metals and Ceramics. Published by Pergamon Press, New York.
Fusseis, F., Regenauer-Lieb, K., Liu, J., Hough, R.M., De Carlo, F., 2009. Creep cavitation can establish a dynamic granular fluid pump in ductile shear zones. Nature 459, 975–977.
Gervilla, F., Proenza, J.A., Frei, R., González-Jiménez, J.M., Garrido, C.J., Melgarejo, J.C., Meibom, A., Díaz-martínez, R., Lavaut, W., 2005. Distribution of platinum-group elements and Os isotopes in chromite ores from Mayarí–Baracoa Ophiolite Belt (eastern Cuba). Contributions to Mineralogy and Petrology 150, 589–607.
Gervilla, F., Padro'n-Navarta, J.A., Kerestedjian, T., Sergeeva, I., González-Jiménez, J.M., Fanlo, I., 2012. Formation of ferrian chromite in podiform chromitites from the Golyamo Kamenyane serpentinite, Eastern Rhodopes, SE Bulgaria: a two stage

process. Contributions to Mineralogy and Petrology http://dx.doi.org/10.1007/s00410-012-0763-3.
Ghisler, M., 1976. The geology, mineralogy and geochemistry of the preorogenic Archaean stratiform chromite deposits at Fiskenaesset, West Greenland. Monograph Series on Mineral Deposits 14, 156.
Ghosh, B., Konar, R., 2012. Textural developments in chromite deforming under eclogitefacies conditions from the Neoarchaean Sittampundi anorthosite complex, southern India. Geological Journal 47, 253–262.
Ghosh, B., Morishita, T., Bhatta, K., 2013. Significance of chromian spinels from the mantle sequence of the Andaman Ophiolite, India: paleogeodynamic implications. Lithos 164–167, 86–96.
Ghosh, B., Ray, J., Morishita, T., 2014. Grain-scale plastic deformation of chromite from podiform chromitite of the Naga–Manipur ophiolite belt, India: implication for mantle dynamics. Ore Geology Reviews 56, 199–208.
González-Jiménez, J.M., Gervilla, F., Griffin, W.L., Proenza, J.A., Augé, T., O'Reilly, S.Y., Pearson, N.J., 2012. Os-isotope variability within sulfides from podiform chromitites. Chemical Geology 291, 224–235.
González-Jiménez, J.M., Griffin, W.L., Proenza, J.A., Gervilla, F., O'Reilly, S.Y., Akbulut, M., Pearson, N.J., Arai, S., 2014. Chromitites in ophiolites: how, where, when, why? Part II. The crystallization of chromitites. Lithos 189, 140–158.
Grewen, J., Huber, L., 1978. In: Gaessner, F. (Ed.), Recrystallization of Metallic Materials. Springer, p. 111.
Halfpenny, A., Prior, D.J., Wheeler, J., 2006. Analysis of dynamic recrystallization and nucleation in a quartzite mylonite. Tectonophysics 427, 3–14.
Haydoutov, I., Kolcheva, K., Dieva, L.A., Savov, I., Carrigan, C., 2004. Island arc origin of the variegated formations from the east Rhodope, Bulgaria — implications for the evolution of the Rhodope Massif. Ofioliti 29 (2), 145–157.
Hennig-Michaeli, C., Siemes, H., 1982. Compression experiments on natural magnetite crystals at 200 °C and 400 °C at 400 MPa confining pressure. In: Goodman, G.E., Heuze, F.E. (Eds.), Issues in Rock Mechanics, Twenty-third Symposium on Rock Mechanics. American Institute of Mining, Metallurgical and Petroleum Engineers, New York, pp. 380–388.
Holness, M.B., Watt, G.R., 2001. Quartz recrystallization and fluid flow during contact metamorphism: a cathodoluminescence study. Geofluids 1, 215–228.
Huang, X., Jianghai, L., Kusky, T.M., Chen, Z., 2004. Microstructures of the Zunhua 2.50 Ga Podiform Chromite, North China Craton and implications for the deformation and rheology of the Archean oceanic lithospheric mantle. In: Kusky, T.M. (Ed.), Precambrian Ophiolites and Related Rocks. Developments in Precambrian Geology 13. Elsevier, Amsterdam, pp. 321–338.
Hull, D., Rimmer, D.E., 1959. The growth of grain-boundary voids under stress. Philosophical Magazine 4 (42), 673–687.
Humphreys, F.J., Fatherly, M., 2004. Recrystallization and Related Annealing Phenomena. Second edition. Elsevier.
Kolcheva, K., Haydoutov, I., Daieval, L., 2000. Dismembered ultramafic ophiolites from the Avren synform, Eastern Rhodopes. Geochemistry, Mineralogy and Petrology 37, 25–38.
Kruse, R., Stünitz, H., 1999. Deformation mechanisms and phase distribution in mafic high-temperature mylonites from the Jotun Nappe, southern Norway. Tectonophysics 303, 223–249.
Kruse, R., Stünitz, H., Kunze, K., 2001. Dynamic recrystallization processes in plagioclase porphyroclasts. Journal of Structural Geology 23, 1781–1802.
Law, R.D., Schmid, S.M., Wheeler, J., 1990. Simple shear deformation and quartz crystallographic fabrics: a possible natural example from the Torridon area of NW Scotland. Journal of Structural Geology 12, 29–46.
Lloyd, G.E., Farmer, A.B., Mainprice, D., 1997. Misorientation analysis and the formation and orientation of subgrain and grain boundaries. Tectonophysics 279, 55–78.
Lloyd, G.E., Freeman, B., 1994. Dynamic recrystallisation of quartz and quartzite. Journal of Structural Geology 16, 867–881.
Mainprice, D., Silver, P.G., 1993. Interpretation of SKS-waves using samples from the subcontinental lithosphere. Physics of the Earth and Planetary Interiors 78, 257–280.
McCaig, A., Covey-Crump, S.J., Ben Ismail, W., Lloyd, G.E., 2007. Fast diffusion along mobile grain boundaries in calcite. Contributions to Mineralogy and Petrology 153, 159–175.
McGowan, N.M., Griffin, W.L., González-Jiménez, J.M., Belousova, E.A., Afonso, J., Shi, R., McCammon, C.A., Pearson, N.J., O'Reilly, S.Y., 2015. Tibetan chromitites: excavating the slab graveyard. Geology 43, 179–182.
Melcher, F., Grum, W., Simon, G., Thalhammer, T.V., Stumpfl, E.F., 1997. Petrogenesis of the ophiolitic giant chromite deposits of Kempirsai, Kazakhstan: a study of solid and fluid inclusions in chromite. Journal of Petrology 38, 1419–1458.
Menegon, L., Piazolo, S., Pennacchioni, G., 2011. The effect of Dauphiné twinning on plastic strain in quartz. Contributions to Mineralogy and Petrology 161, 635–652.
Menegon, L., Fusseis, F., Stünitz, H., Xianghui Xiao, X., 2015. Creep cavitation bands control porosity and fluid flow in lower crustal shear zones. Geology 43, 227–230.
Miura, M., Arai, S., Ahmed, A.H., Mizukami, T., Okuno, M., Yamamoto, S., 2012. Podiform chromitite classification revisited: a comparison of discordant and concordant chromitite pods from Wadi Hilti, northern Oman ophiolite. Journal of Asian Earth Sciences 59, 52–61.
Montagnat, M., Blackford, J.R., Piazolo, S., Amaud, L., Lebensohn, R.A., 2011. Measurement and full-field predictions of deformation heterogeneities in ice. Earth and Planetary Science Letters 305, 153–160.
Mposkos, E., 2002. Petrology of the ultrahigh pressure metamorphic Kimi complex in Rhodope (NE Greece): a new insight into the Alpine geodynamic evolution of the Rhodope. Bulletin of the Geological Society of Greece 34, 2126–2188.
Mposkos, E., Krohe, A., 2006. Pressure–temperature–deformation paths of closely associated ultra-high-pressure (diamond-bearing) crustal and mantle rocks of the Kimi complex: implications for the tectonic history of the Rhodope Mountains, northern Greece. Canadian Journal of Earth Sciences 43, 1755–1776.
Mposkos, E., Baziotis, L., Proyer, A., 2011. Pressure–temperature evolution of eclogites from the Kechros complex in the Eastern Rhodope (NE Greece). International Journal of Earth Sciences 101 (4), 973–996.
Müller, P., Siemes, H., 1972. Zur Festigkeit und Gefügeregelung von experimentell verformten Magnetiterzen (Strength and preferred orientation of experimentally deformed magnetite ores). Neues Jahrbuch fur Mineralogie, Abhandlungen 117, 39–60.
Ozawa, K., 1989. Stress-induced Al–Cr zoning of spinel in deformed peridotites. Nature 338, 141–144.
Passchier, C.W., Trouw, R.A.J., 2005. Microtectonics. 2nd edition. Springer, Berlin Heidelberg, New York.
Pearce, M.A., Wheeler, J., 2010. Modelling grain-recycling zoning during metamorphism. Journal of Metamorphic Geology 28 (4), 423–437.
Piazolo, S., Jaconelli, P., 2013. Sillimanite deformation mechanisms within a Grt–Sil–Bt gneiss: effect of pre-deformation grain orientations and characteristics on mechanism, slip-system activation and rheology. In: Llana-Funez, S., Marcos, A., Bastida, F. (Eds.), Deformation Structures and Processes Within the Continental Crust. Geological Society, London, Special Publications, p. 394.
Piazolo, S., Montagnat, M., Blackford, J.R., 2008. Sub-structure characterization of experimentally and naturally deformed ice using cryo-EBSD. Journal of Microscopy 230, 509–519.
Piazolo, S., Austrheim, H., Whitehouse, M., 2012. Brittle–ductile microfabrics in naturally deformed zircon: deformation mechanisms and consequences for U–Pb dating. American Mineralogist 97, 1544–1563.
Prichard, H.M., Barnes, S.J., Godel, B., Reddy, S.M., Vukmanovic, Z., Halfpenny, A., Neary, C.R., Fisher, P.C., 2015. The structure of and origin of nodular chromite from the Troodos ophiolite, Cyprus, revealed using high-resolution X-ray computed tomography and electron backscatter diffraction. Lithos 218–219, 87–98.
Prior, D.J., Boyle, A.P., Brenker, F., Cheadle, M.C., Day, A., Lopez, G., Peruzzo, L., Potts, G.J., Reddy, S.M., Spiess, R., Timms, N.E., Trimby, P.W., Wheeler, J., Zetterström, L., 1999. The application of electron backscatter diffraction and orientation contrast imaging in the SEM to textural problems in rocks. American Mineralogist 84, 1741–1759.
Prior, D.J., Wheeler, J., Peruzzo, L., Spiess, R., Storey, C., 2002. Some garnet micro structures: an illustration of the potential of orientation maps and misorientation analysis in microstructural studies. Journal of Structural Geology 24, 999–1011.
Proenza, J.A., Gervilla, F., Melgarejo, J.C., Bodinier, J.L., 1999. Al- and Cr-rich chromitites from the Mayarí–Baracoa Ophiolitic Belt (Eastern Cuba): consequence of interaction between volatile-rich melts and peridotites in suprasubduction mantle. Economic Geology 94, 547–566.
Putnis, A., 2009. Mineral replacement reactions. Reviews in Mineralogy and Geochemistry 70, 87–124.
Reddy, S.M., Timms, N.E., Pantleon, W., Trimby, P., 2007. Quantitative characterization of plastic deformation of zircon and geological implications. Contributions to Mineralogy and Petrology 153, 625–645.
Rybacki, E., Wirth, R., Dresen, G., 2008. High-strain creep of feldspar rocks: implications for cavitation and ductile failure in the lower crust. Geophysical Research Letters 35, L04304. http://dx.doi.org/10.1029/2007GL032478.
Secher, D., 1981, Les lherzolites ophiolitiques de Nouvelle-Calédonie et leurs gisements de chromite - deformation de la chromite. Unpublished 3me cycle thesis, University of Nantes.
Stipp, M., Stünitz, H., Heilbronner, R., Schmid, S.M., 2002. The eastern Tonale fault zone: a "natural laboratory" for crystal plastic deformation of quartz over a temperature range from 250 to 700 °C. Journal of Structural Geology 24, 1861–1884.
Stowe, C.W., 1994. Compositions and tectonic settings of chromite deposits through time. Economic Geology 89, 528–546.
Svahnberg, H., Piazolo, S., 2012. The initiation of strain localisation in plagioclase-rick rocks: insights from detailed microstructural analyses. Journal of Structural Geology 32 (10), 1404–1416.
Till, J.L., Moskowitz, B., 2013. Magnetite deformation mechanism maps for better prediction of strain partitioning. Geophysical Research Letters 40, 697–702. http://dx.doi.org/10.1002/GRL.50170.
Timms, N.E., Kinny, P.D., Reddy, S.M., 2006. Enhanced diffusion of Uranium and Thorium linked to crystal plasticity in zircon. Geochemical Transactions 7 (10), 1–16.
Timms, N.E., Reddy, S.M., FitzGerald, J.D., Green, L., Muhling, J.R., 2012. Inclusion-localised crystal-plasticity, dynamic porosity, and fast-diffusion pathway generation in zircon. Journal of Structural Geology 35, 78–89.
Trimby, P.W., Prior, D.J., Wheeler, J., 1998. Grain boundary hierarchy development in a quartz mylonite. Journal of Structural Geology 20, 913–935.
Urai, J., Means, W.D., Lister, G.S., 1986. Dynamic recrystallization of minerals. In: Heard, H.C., Hobbs, B.E. (Eds.), Mineral and Rock Deformation: Laboratory Studies, the Paterson Volume. Geophys. Monogr 36. Am. Geophys. Union, Washington DC, pp. 161–200.
Vukmanovic, Z., Barnes, S.J., Reddy, S.M., Godel, B., Fiorentini, M.L., 2013. Morphology and microstructure of chromite crystals in chromitites from the Merensky Reef (Bushveld Complex, South Africa). Contributions to Mineralogy and Petrology 165, 1031–1050.
Walker, R.J., Prichard, H.M., Ishiwatari, A., Pimentel, M., 2002. The osmium isotopic composition of convecting upper mantle deduced from ophiolite chromites. Geochimica et Cosmochimica Acta 66, 329–345.
Wheeler, L., 2009. The preservation of seismic anisotropy in the Earth's mantle during diffusion creep. Geophysical Journal International 178, 1723–1732.
Yund, R.A., Tullis, J., 1991. Compositional changes of minerals associated with dynamic recrystallisation. Contributions to Mineralogy and Petrology 108, 346–355.
Zhou, M.F., Robinson, P.T., Bai, W.J., 1994. Formation of podiform chromitites by melt/rock interaction in the upper mantle. Mineral Deposits 29, 98–101.
Zhou, M.F., Robinson, P., Malpas, J., Li, Z., 1996. Podiform chromites in the Luobusa ophiolite (Southern Tibet): implications for melt rock interaction and chromite segregation in the upper mantle. Journal of Petrology 37, 3–21.